

# Production of $a_0$ -mesons in $pp$ and $pn$ reactions <sup>\*</sup>

E.L. Bratkovskaya <sup>a</sup>, V. Yu. Grishina <sup>b,c</sup>, L.A. Kondratyuk <sup>c,d</sup>, M. Büscher <sup>d</sup>, and W. Cassing <sup>a</sup>

<sup>a</sup> Institut für Theoretische Physik, Universität Giessen, D-35392 Giessen, Germany

<sup>b</sup> Institute for Nuclear Research, 60th October Anniversary Prospect 7A, 117312 Moscow, Russia

<sup>c</sup> Institute of Theoretical and Experimental Physics, B.Chernushkinskaya 25, 117259 Moscow, Russia

<sup>d</sup> Institut für Kernphysik, Forschungszentrum Jülich, D-52425 Jülich, Germany

Received: date / Revised version: date

**Abstract.** We investigate the cross section for the reaction  $NN \rightarrow NN a_0$  near threshold and at medium energies. An effective Lagrangian approach with one-pion exchange is applied to analyze different contributions to the cross section for different isospin channels. The Reggeon exchange mechanism is also considered. The results are used to calculate the contribution of the  $a_0$  meson to the cross sections and invariant  $K\bar{K}$  mass distributions of the reactions  $pp \rightarrow pnK^+\bar{K}^0$  and  $pp \rightarrow ppK^+K^-$ . It is found that the experimental observation of  $a_0^+$  mesons in the reaction  $pp \rightarrow pnK^+\bar{K}^0$  is much more promising than the observation of  $a_0^0$  mesons in the reaction  $pp \rightarrow ppK^+K^-$ .

**PACS.** 25.10.+s Meson production – 13.75.-n Proton induced reactions

## 1 Introduction

The excitations of the QCD vacuum with different quantum numbers as well as their life times and decay modes are of fundamental interest in the physics of the strong interaction. The masses of the pseudo-scalar mesons have been found to be essentially due to a spontaneous breaking of the chiral  $SU(3)_R \times SU(3)_L$  symmetry or the  $U(1)_A$  anomaly (in case of the  $\eta'$ ). The vector mesons  $\rho$ ,  $\omega$ ,  $\phi$ ,  $K^*$ ,  $J/\Psi$  etc., which are the dipole modes of the vacuum, have found increasing attention during the last two decades. Especially their decay to dileptons is presently investigated in elementary and complex (nucleus-nucleus) collisions in different laboratories all over the world (cf. the reviews [1,2,3] and Refs. therein). On the other hand, the scalar sector of vacuum excitations is not well known experimentally and theoretically, so far.

The structure of the lightest scalar mesons  $a_0(980)$  and  $f_0(980)$ , that carry the quantum numbers of the QCD vacuum, is still under discussion (see e.g. [4,5,6,7,8,9,10] and references therein). Different authors interpreted them as unitarized  $q\bar{q}$  states or as four-quark cryptoexotic states or as  $K\bar{K}$  molecules or even as vacuum scalars (Gribov's minions). Although it has been possible to describe them as ordinary  $q\bar{q}$ -states (see Refs.[11,12,13]), other options cannot be ruled out up to now. Another problem is the possible strong mixing between the uncharged  $a_0(980)$  and the  $f_0(980)$  due to a common coupling to  $K\bar{K}$  intermediate states [14,15,16,17,18,19,20]. This effect can influence

the structure of the uncharged component of the  $a_0(980)$  and implies that it is important to perform a comparative study of  $a_0^0$  and  $a_0^+$  (or  $a_0^-$ ). There is no doubt that new data on  $a_0^0$  and  $a_0^+/a_0^-$  production in  $\pi N$  and  $NN$  reactions are quite important to shed new light on the  $a_0$  structure and the dynamics of its production.

If the  $a_0$  meson is an ordinary  $q\bar{q}$  state, it is expected that the cross section of its production in photon, pion and proton beams is about  $\simeq 1/6$  of the  $\rho$ -meson non-diffractive production cross section (see e.g. Refs. [21,22]). In our recent paper [22] we have considered  $a_0$  production in the reaction  $\pi N \rightarrow a_0 N$  near the threshold and at GeV energies. An effective Lagrangian approach as well as the Regge pole model were applied to investigate different contributions to the cross-section of the reaction  $\pi N \rightarrow a_0 N$ . Here we employ the latter results for an analysis of  $a_0$  production in  $NN$  collisions. Our study is particularly relevant to the current experimental program at COSY-Jülich [23,24,25].

Our paper is organized as follows: In Sect. 2 we discuss an effective Lagrangian approach with one-pion exchange while the Reggeon exchange model is considered in Sect. 3. Sect. 4 is devoted to the calculations of the cross section for the reaction  $NN \rightarrow NN a_0$ . In Sect. 5 we analyze the contribution of the  $a_0$  resonance to the cross sections and invariant  $K\bar{K}$  mass distributions for the reactions  $pp \rightarrow ppK^+K^-$  and  $pp \rightarrow pnK^+\bar{K}^0$ . Our conclusions are presented in Sect. 6.

<sup>\*</sup> Supported by Forschungszentrum Jülich, DFG and RFFI

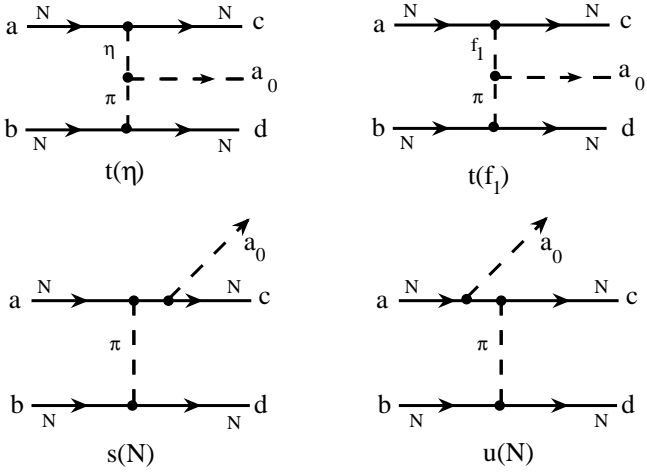


**Fig. 1.** Diagrams for  $a_0$  production in the reaction  $NN \rightarrow a_0NN$  near threshold as considered in the present study.

## 2 An effective Lagrangian approach with one-pion exchange

We consider  $a_0^0$ ,  $a_0^+$ ,  $a_0^-$  production in the reactions  $j = pp \rightarrow pp a_0^0$ ,  $pp \rightarrow pn a_0^+$ ,  $pn \rightarrow pp a_0^-$  and  $pn \rightarrow pn a_0^0$  using the effective Lagrangian approach with one-pion exchange (OPE). For the elementary  $\pi N \rightarrow N a_0$  transition amplitude we take into account different mechanisms  $\alpha$  corresponding to  $t$ -channel diagrams with  $\eta(550)$ - and  $f_1(1285)$ -meson exchanges ( $\alpha = t(\eta)$ ,  $t(f_1)$ ) as well as  $s$ - and  $u$ -channel graphs with an intermediate nucleon ( $\alpha = s(N)$ ,  $u(N)$ ) (cf. Ref. [22]). The corresponding diagrams are shown in Fig. 1. The invariant amplitude of the  $NN \rightarrow NN a_0$  reaction then is the sum of the four basic terms (diagrams in Fig. 1) with permutations of nucleons in the initial and final states

$$\begin{aligned} \mathcal{M}_{j(\alpha)}^\pi[ab; cd] & \\ &= \xi_{j(\alpha)}^\pi[ab; cd] \mathcal{M}_\alpha^\pi[ab; cd] + \xi_{j(\alpha)}^\pi[ab; dc] \mathcal{M}_\alpha^\pi[ab; dc] \\ &+ \xi_{j(\alpha)}^\pi[ba; dc] \mathcal{M}_\alpha^\pi[ba; dc] + \xi_{j(\alpha)}^\pi[ba; cd] \mathcal{M}_\alpha^\pi[ba; cd], \end{aligned} \quad (1)$$

where the coefficients  $\xi_{j(\alpha)}^\pi$  are given in Table 1. The amplitude for the  $t$ -channel exchange with  $\eta(550)$ - and  $f_1(1285)$ -mesons are given by

$$\begin{aligned} \mathcal{M}_{t(\eta)}^\pi[ab; cd] &= g_{a_0\eta\pi} F_{a_0\eta\pi} ((p_a - p_c)^2, (p_d - p_b)^2) \\ &\times g_{\eta NN} F_{\eta NN} ((p_a - p_c)^2) \frac{1}{(p_a - p_c)^2 - m_\eta^2} \\ &\times \bar{u}(p_c) \gamma_5 u(p_a) \times \Pi(p_b; p_d), \end{aligned} \quad (2)$$

$$\begin{aligned} \mathcal{M}_{t(f_1)}^\pi[ab; cd] &= -g_{a_0 f_1 \pi} F_{a_0 f_1 \pi} ((p_a - p_c)^2, (p_d - p_b)^2) \\ &\times g_{f_1 NN} F_{f_1 NN} ((p_a - p_c)^2) \frac{1}{(p_a - p_c)^2 - m_{f_1}^2} \\ &\times (p_a - p_c + 2(p_b - p_d))_\mu \left( g_{\mu\nu} - \frac{(p_a - p_c)_\mu (p_a - p_c)_\nu}{m_{f_1}^2} \right) \\ &\times \bar{u}(p_c) \gamma_5 \gamma_\nu u(p_a) \times \Pi(p_b; p_d), \end{aligned} \quad (3)$$

with

$$\begin{aligned} \Pi(p_b; p_d) &= \frac{f_{\pi NN}}{m_\pi} F_{\pi NN} ((p_b - p_d)^2) (p_b - p_d)_\beta \\ &\times \bar{u}(p_d) \gamma_5 \gamma_\beta u(p_b) \frac{1}{(p_b - p_d)^2 - m_\pi^2}. \end{aligned} \quad (4)$$

The amplitudes for the  $s$ - and  $u$ -channels (lower part of Fig. 1) are given as

$$\begin{aligned} \mathcal{M}_{s(N)}^\pi[ab; cd] &= \Pi(p_b; p_d) \frac{f_{\pi NN}}{m_\pi} F_{\pi NN} ((p_d - p_b)^2) \\ &\times g_{a_0 NN} \frac{F_{a_0 NN} ((p_a + p_b - p_d)^2)}{(p_a + p_b - p_d)^2 - m_N^2} (p_d - p_b)_\mu \\ &\times \bar{u}(p_c) [(p_a + p_b - p_d)_\delta \gamma_\delta + m_N] \gamma_5 \gamma_\mu u(p_a), \end{aligned} \quad (5)$$

$$\begin{aligned} \mathcal{M}_{u(N)}^\pi[ab; cd] &= \Pi(p_b; p_d) \frac{f_{\pi NN}}{m_\pi} F_{\pi NN} ((p_d - p_b)^2) \\ &\times g_{a_0 NN} \frac{F_{a_0 NN} ((p_c + p_d - p_b)^2)}{(p_c + p_d - p_b)^2 - m_N^2} (p_d - p_b)_\mu \\ &\times \bar{u}(p_c) \gamma_5 \gamma_\mu [(p_c + p_d - p_b)_\delta \gamma_\delta + m_N] u(p_a). \end{aligned} \quad (6)$$

Here  $p_a, p_b$  and  $p_c, p_d$  are the four momenta of the initial and final nucleons, respectively.

The  $\pi NN$  coupling constant is taken as  $f_{\pi NN}^2/4\pi = 0.08$  [26] and the form factor for each virtual nucleon is taken in the form [27]

$$F_{a_0 NN}(u) = \frac{\Lambda_{a_0 NN}^4}{\Lambda_{a_0 NN}^4 + (u - m_N^2)^2} \quad (7)$$

with a cut-off parameter  $\Lambda_{a_0 NN} = 1.24$  GeV. The coupling constant  $g_{a_0 NN}^2/4\pi = 1.075$  is taken from Ref. [28].

The functions  $F_i$  represent form factors at the different vertices  $i$  ( $i = \pi NN, \eta NN, f_1 NN$ ), which are taken of the monopole form,

$$F_i(t) = \frac{\Lambda_i^2 - m_i^2}{\Lambda_i^2 - t}, \quad (8)$$

where  $\Lambda_i$  is a cut-off parameter.

For  $\pi$  exchange we use  $\Lambda_{\pi NN} = 1.05 \div 1.3$  GeV. In the case of  $\eta$  exchange we use  $g_{\eta NN}^2/4\pi = 3$ ,  $\Lambda_{\eta NN} = 1.5$  GeV from Ref. [26] and  $g_{a_0 \eta \pi} = 2.46$  GeV, which results from the width  $\Gamma(a_0 \rightarrow \eta\pi) = 80$  MeV.

The contribution of the  $f_1$  exchange is calculated with  $g_{f_1 NN} = 11.2$ ,  $\Lambda_{f_1 NN} = 1.5$  GeV from Ref. [29] and  $g_{a_0 f_1 \pi} = 2.5$ . The latter value for  $g_{a_0 f_1 \pi}$  corresponds to  $\Gamma(f_1 \rightarrow a_0 \pi) = 24$  MeV and  $Br(f_1 \rightarrow a_0 \pi) = 34\%$ . The same parameters have been used in our previous study of  $a_0$  production in  $\pi N \rightarrow a_0 N$  and  $pp \rightarrow da_0^+$  reactions [22].

For the form factors at the  $a_0 f_1 \pi$  (as well as  $a_0 \eta \pi$ ) vertex factorized forms are applied following the assumption from Refs. [30,31]

$$F_{a_0 f_1 \pi}(t_1, t_2) = F_{f_1 NN}(t_1) F_{\pi NN}(t_2), \quad (9)$$

where  $F_{f_1 NN}(t), F_{\pi NN}(t)$  are taken as in (8).

Reaction $j$ (mechanism $\alpha$ )	$\xi_{j(\alpha)}^\pi[ab; cd]$	$\xi_{j(\alpha)}^\pi[ab; dc]$	$\xi_{j(\alpha)}^\pi[ba; dc]$	$\xi_{j(\alpha)}^\pi[ba; cd]$
$pp \rightarrow ppa_0^0$ ( $t(\eta), t(f_1)$ )	$+1/\sqrt{2}$	$-1/\sqrt{2}$	$+1/\sqrt{2}$	$-1/\sqrt{2}$
( $s(N)$ )	$+1/\sqrt{2}$	$-1/\sqrt{2}$	$+1/\sqrt{2}$	$-1/\sqrt{2}$
( $u(N)$ )	$+1/\sqrt{2}$	$-1/\sqrt{2}$	$+1/\sqrt{2}$	$-1/\sqrt{2}$
Regge	0	0	0	0
$pp \rightarrow pna_0^+$ ( $t(\eta), t(f_1)$ )	$-\sqrt{2}$	0	0	$+\sqrt{2}$
( $s(N)$ )	0	$+\sqrt{2}$	$-\sqrt{2}$	0
( $u(N)$ )	$+2\sqrt{2}$	$-\sqrt{2}$	$+\sqrt{2}$	$-2\sqrt{2}$
Regge	-1	+1	-1	+1
$pn \rightarrow ppa_0^-$ ( $t(\eta), t(f_1)$ )	+1	-1	0	0
( $s(N)$ )	-2	+2	-1	+1
( $u(N)$ )	0	0	+1	-1
Regge	$+1/\sqrt{2}$	$-1/\sqrt{2}$	$-1/\sqrt{2}$	$+1/\sqrt{2}$
$pn \rightarrow pna_0^0$ ( $t(\eta), t(f_1)$ )	-1	0	+1	0
( $s(N)$ )	-1	-2	+1	+2
( $u(N)$ )	-1	+2	+1	-2
Regge	0	$+\sqrt{2}$	0	$-\sqrt{2}$

**Table 1.** Coefficients in Eq. (1) for different mechanisms of the  $pp \rightarrow ppa_0^0$ ,  $pp \rightarrow ppa_0^+$ ,  $pn \rightarrow ppa_0^-$  and  $pn \rightarrow pna_0^0$  reactions.

The total cross section for  $a_0$  production in the isospin reaction  $j$  is given as the coherent sum of the amplitudes (1) over all channels ( $\alpha = s(N), u(N), t(f_1), t(\eta)$ ) integrated over phase space

$$\sigma_{a_0}^j(s) = \int dE_c dq_0 d\cos\theta_q d\varphi_q \frac{1}{2^9 \pi^4 p_a \sqrt{s}} \times \left| \sum_{\alpha} \mathcal{M}_{j(\alpha)}^\pi[ab; cd] \right|^2. \quad (10)$$

Here  $s = (p_a + p_b)^2$  is the total energy of the  $NN$  system squared,  $E_c$  and  $q_0$  are the energy of the outgoing nucleon and  $a_0$  meson, respectively.  $\theta_q$  is the polar angle of the 3-momentum of the  $a_0$ -meson  $\mathbf{q}$  in the cms of the initial nucleons defined as  $\theta_q = \mathbf{q}, \widehat{\mathbf{p}_a}$ , while  $\varphi_q$  is the azimuthal angle of  $\mathbf{q}$  in the cms.

As shown in the analysis in Ref. [22] the contribution of the  $\eta$ -exchange to the amplitude  $\pi N \rightarrow a_0 N$  is small. Note that in Ref. [32] only this mechanism was taken into account for the reaction  $pn \rightarrow ppa_0^-$ . Here we also include the  $\eta$ -exchange because it might be noticeable in those isospin channels where a strong destructive interference of  $u$ - and  $s$ -channel terms can occur (see below).

### 3 The Reggeon exchange model

Here as in Ref. [22] we use the Regge-pole model for the amplitude  $\pi N \rightarrow a_0 N$  as developed by Achasov and Shestakov [15]. The  $s$ -channel helicity amplitudes for the reaction  $\pi^- p \rightarrow a_0^0 n$  in this approach can be written as

$$M_{\lambda_2' \lambda_2}(\pi^- p \rightarrow a_0^0 n) = \bar{u}_{\lambda_2'}(p_2') [-A(s, t) + (p_1 + p_1')_\alpha \gamma_\alpha \frac{B(s, t)}{2}] \gamma_5 u_{\lambda_2}(p_2), \quad (11)$$

where the invariant amplitudes  $A(s, t)$  and  $B(s, t)$  do not contain kinematical singularities. The relations between

the invariant and  $s$ -wave helicity amplitudes are given by

$$M_{++} = -M_{--} \quad (12)$$

$$= \cos \frac{\theta}{2} [A(s, t) \sqrt{-t_{min}} - B(s, t) \sqrt{-t_{max} s}],$$

$$M_{+-} = M_{-+} \quad (13)$$

$$= \cos \frac{\theta}{2} [A(s, t) \sqrt{-t_{max}} - B(s, t) \sqrt{-t_{min} s}],$$

where  $\theta$  is the c.m. scattering angle, while  $t_{min}$  and  $t_{max}$  are the values of  $t$  at  $\theta=0^\circ$  and  $180^\circ$ , respectively.

In the model of Ref. [15] the  $s$ -channel helicity amplitudes are expressed through the  $b_1$  and the conspiring  $\rho_2$  Regge trajectories exchange as follows

$$M_{++} = \gamma_{\rho_2}(t) \exp \left[ -i \frac{\pi}{2} \alpha_{\rho_2}(t) \right] \left( \frac{s}{s_0} \right)^{\alpha_{\rho_2}(t)}, \quad (14)$$

$$M_{+-} = \sqrt{(t_{min} - t)/s_0} \gamma_{b_1}(t) \times i \exp \left[ -i \frac{\pi}{2} \alpha_{b_1}(t) \right] \left( \frac{s}{s_0} \right)^{\alpha_{b_1}(t)}. \quad (15)$$

As in Ref. [22] we take the meson Regge trajectories in linear form  $\alpha_j(t) = \alpha_j(0) + \alpha_j'(0)t$  with  $\alpha_{b_1}(0) \simeq -0.37$ ,  $\alpha_{\rho_2}(0) \simeq -0.6$  and  $\alpha_{b_1}'(0) = \alpha_{\rho_2}'(0) = 0.9 \text{ GeV}^{-2}$ . The residues are parametrized in a conventional way,  $\gamma_{\rho_2}(t) = \gamma_{\rho_2}(0) \exp(b_{\rho_2} t)$ ,  $\gamma_{b_1}(t) = \gamma_{b_1}(0) \exp(b_{b_1} t)$ ; all parameters were taken the same as in Ref. [22]. They correspond to two fits of the Brookhaven data on  $d\sigma/dt$  at 18 GeV/c [33] found by Achasov and Shestakov [15]: a) with pure  $\rho_2$  contribution and b) with combined  $\rho_2 + b_1$  contribution.

The invariant amplitude corresponding to the diagram of Fig. 2 can be written as

$$\mathcal{M}_{Regge}^\pi[ab; cd] = \bar{u}(p_c) [-A(s, t)$$

$$\begin{aligned}
& + (p_{a_0} + p_d - p_b)_\alpha \gamma_\alpha \frac{B(s, t)}{2} \Big] \gamma_5 u(p_a) \\
& \times \bar{u}(p_d) \gamma_5 u(p_b) \times \Pi(p_b; p_d).
\end{aligned} \tag{16}$$

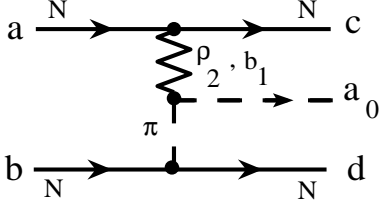


**Fig. 2.** The diagram for  $a_0$  production in the reaction  $NN \rightarrow NN a_0$  within the Regge exchange model.

#### 4 The reaction $NN \rightarrow NN a_0$

In order to demonstrate the sensitivity of the OPE model to the cut-off parameter  $\Lambda_{\pi NN}$  used in the  $\pi NN$  vertices we show in Fig. 3 the total cross section for the reaction  $pp \rightarrow pna_0^+$  for  $u(N)$  and  $t(f_1)$  channels as a function of the excess energy  $Q = \sqrt{s} - \sqrt{s_0}$ , where  $\sqrt{s_0} = m_{a_0} + 2m_N$ , calculated for different cut-off parameters. The dotted lines correspond to  $\Lambda_{\pi NN} = 0.8$  GeV, the solid lines show the result for  $\Lambda_{\pi NN} = 1.05$  GeV whereas the dashed lines indicate  $\Lambda_{\pi NN} = 1.3$  GeV. The results for  $\Lambda_{\pi NN} = 1.3$  GeV and 0.8 GeV differ by a factor of  $\sim 5$ . For our subsequent calculation we choose  $\Lambda_{\pi NN} = 1.05$  GeV while keeping the uncertainty on  $\Lambda_{\pi NN}$  in mind.

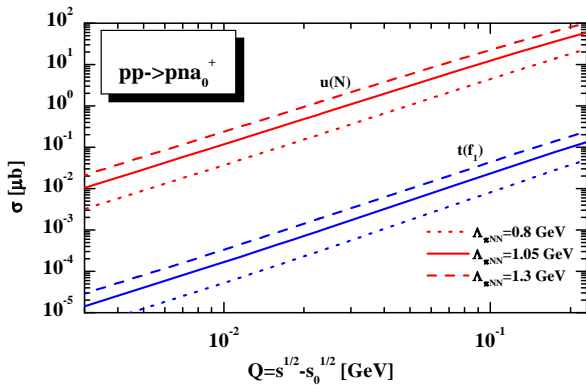


**Fig. 3.** The total cross section for the reaction  $pp \rightarrow pna_0^+$  for  $u(N)$  and  $t(f_1)$  channels as a function of the excess energy  $Q = \sqrt{s} - \sqrt{s_0}$  for different cut-off parameters  $\Lambda_{\pi NN} = 0.8$  GeV (dotted lines),  $\Lambda_{\pi NN} = 1.05$  GeV (solid lines) and  $\Lambda_{\pi NN} = 1.3$  GeV (dashed lines).

Since we have two nucleons in the final state it is necessary to take into account their final-state-interaction (FSI), which has some influence on meson production near threshold. For this purpose we adopt the FSI model from

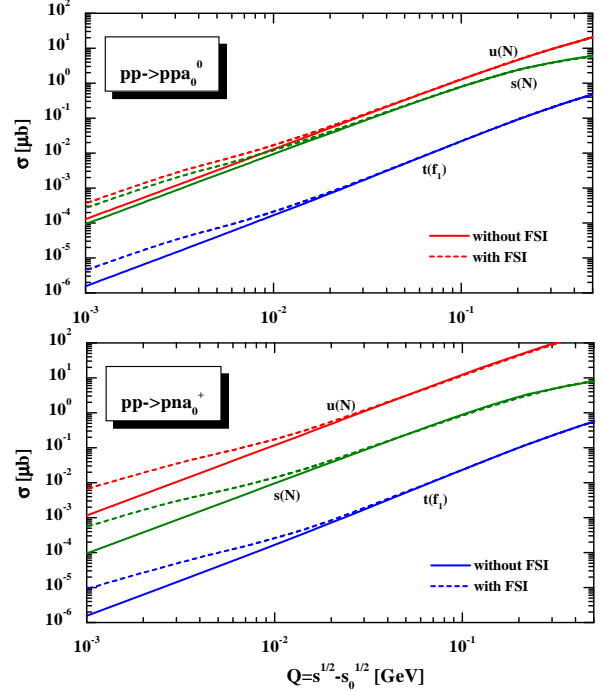


**Fig. 4.** The total cross section for the reactions  $pp \rightarrow ppa_0^0$  (upper part) and  $pp \rightarrow pna_0^+$  (lower part) as a function of the excess energy  $Q = \sqrt{s} - \sqrt{s_0}$  for  $u(N)$ ,  $s(N)$  and  $t(f_1)$  channels calculated without FSI (solid lines) and with FSI (dashed lines).

Ref. [34] based on the (realistic) Paris potential. We use, however, the enhancement factor  $F_{NN}(q_{NN})$  – as given by this model – only in the region of small relative momenta of the final nucleons  $q_{NN} \leq q_0$ , where it is larger than 1. Having in mind that this factor is rather uncertain at larger  $q_{NN}$ , where for example contributions of nonnucleon intermediate states to the loop integral might be important, we assume that  $F_{NN}(q_{NN}) = 1$  for  $q_{NN} \geq q_0$ .

In Fig. 4 we show the FSI effect on the total cross section for the reactions  $pp \rightarrow ppa_0^0$  (upper part) and  $pp \rightarrow pna_0^+$  (lower part) for  $u(N)$ ,  $s(N)$  and  $t(f_1)$  channels. The solid lines show the calculation without FSI whereas the dashed lines indicate the results with FSI. As seen from Fig. 4, the FSI effect is stronger for  $pn$  than for  $pp$  in the final state due to the Coulomb repulsive interaction in the  $pp$  system and the isospin dependence of the  $NN$  interaction at small relative momenta.

The results of our calculations for the total cross sections with FSI for the different isospin reactions are presented in Figs. 5, 6 as a function of  $Q = \sqrt{s} - \sqrt{s_0}$ . In Fig. 5 we show the total cross section for the  $pp$  reactions –  $pp \rightarrow ppa_0^0$  (upper part) and  $pp \rightarrow pna_0^+$  (lower part), whereas in Fig. 6 we display the results for the  $pn$  reactions –  $pn \rightarrow ppa_0^-$  (upper part) and  $pn \rightarrow pna_0^0$  (lower part). The solid lines with full dots and with open squares represent the results within the  $\rho_2$  and  $(\rho_2, b_1)$  Regge exchange model. The short dotted lines corresponds to the  $t(f_1)$  channel, the dotted lines to the  $t(\eta)$  channel, the

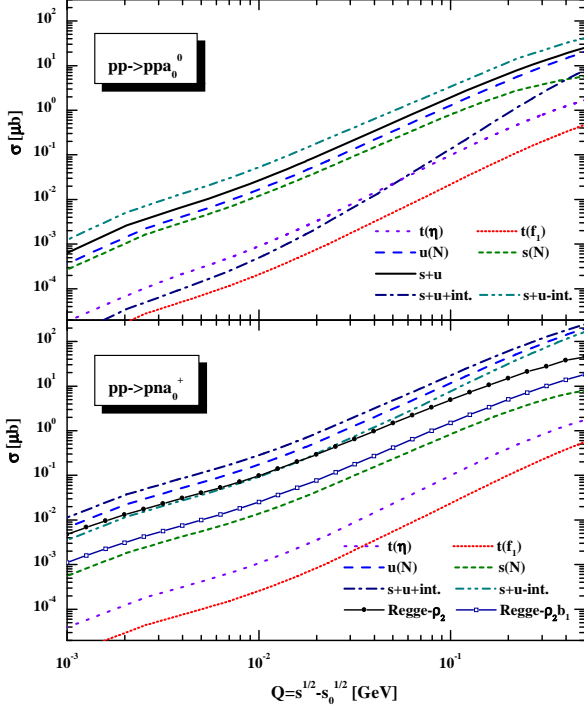


**Fig. 5.** The total cross sections for the reactions  $pp \rightarrow ppa_0^0$  (upper part) and  $pp \rightarrow pna_0^+$  (lower part) as a function of the excess energy  $Q = \sqrt{s} - \sqrt{s_0}$  calculated with FSI. The short dotted lines corresponds to the  $t(f_1)$  channel, the dotted lines to the  $t(\eta)$  channel, the dashed lines to the  $u(N)$  channel, the short dashed lines to the  $s(N)$  channel. The solid line is the incoherent sum of the contributions from  $s(N)$  and  $u(N)$  channels ( $s + u$ ). The dot-dashed lines indicate the coherent sum of  $s(N)$  and  $u(N)$  channels with 'plus' interference ( $s + u + int.$ ), the dot-dot-dashed lines with 'minus' interference ( $s + u - int.$ ). The solid lines with full dots and with open squares present the results within the  $\rho_2$  and  $(\rho_2, b_1)$  Regge exchange model.

dashed lines to the  $u(N)$  channel, the short dashed lines to the  $s(N)$  channel. The solid line in the upper part of Fig. 5 is the incoherent sum of the contributions from  $s(N)$  and  $u(N)$  channels ( $s + u$ ).

As seen from the plots, the  $u$ - and  $s$ -channels give the dominant contribution; the  $t(f_1)$  channel is small for all isospin reactions. For  $pp \rightarrow pna_0^+$ ,  $pn \rightarrow ppa_0^-$  and  $pn \rightarrow pna_0^0$  the Regge exchange contribution (extended to low energies) becomes important and for the  $pn \rightarrow pna_0^0$  reaction this contribution is even dominant near threshold. For the  $pp \rightarrow ppa_0^0$  channel the Regge model predicts no contribution from  $\rho_2$  and  $\rho_2, b_1$  exchanges due to isospin arguments, thus only  $s$ -,  $u$ - and  $t(f_1)$ - channels are plotted in the upper part of Fig. 5.

Here we have to point out the influence of the interference between the  $s$ - and  $u$ -channels. According to the isospin coefficients from the OPE model presented in Table 1, the phase (of interference  $\alpha$ ) between the  $s$ - and  $u$ -channels  $\mathcal{M}_{s(N)}^\pi + \exp(-i\alpha)\mathcal{M}_{u(N)}^\pi$  is equal to zero, i.e. the sign between  $\mathcal{M}_{s(N)}^\pi$  and  $\mathcal{M}_{u(N)}^\pi$  is 'plus'. The dot-dashed

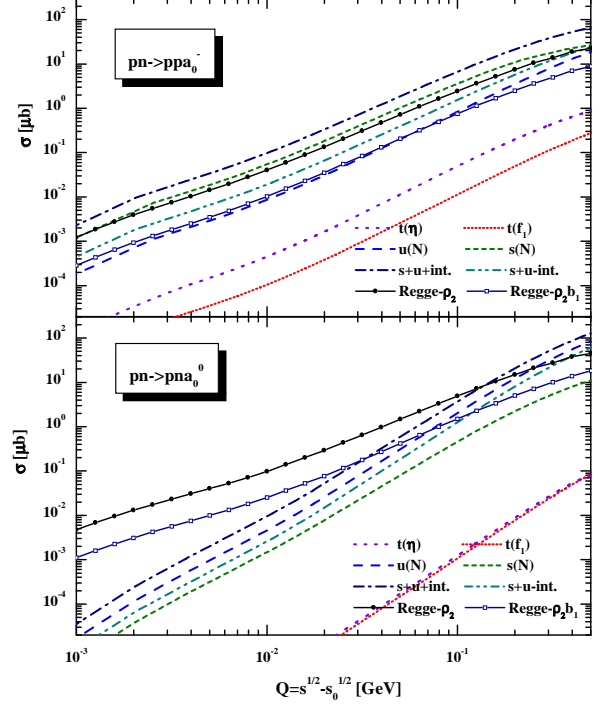


**Fig. 6.** The total cross sections for the reactions  $pn \rightarrow ppa_0^-$  (upper part) and  $pn \rightarrow pna_0^0$  (lower part) as a function of  $Q = \sqrt{s} - \sqrt{s_0}$  calculated with FSI. The assignment of the individual lines is the same as in Fig. 5.

lines in Figs. 5, 6 indicate the coherent sum of  $s(N)$  and  $u(N)$  channels with 'plus' interference ( $s + u + int.$ ). One can see that for  $pp \rightarrow pna_0^+$ ,  $pn \rightarrow ppa_0^-$  and  $pn \rightarrow pna_0^0$  reactions the interference is positive and increases the cross section, whereas for the  $pp \rightarrow ppa_0^0$  channel the interference is strongly destructive since we have identical particles in the initial and final states and the contributions of  $s$ - and  $u$ -channels are very similar.

Note, that the extension of our OPE (one-pion-exchange) model to the OBE (one-boson-exchange), i.e. accounting for the exchange of  $\sigma, \rho, \omega, \dots$  mesons (or other waves in the  $NN$  interaction) would change the isospin coefficients  $\xi_{j(\alpha)}^\pi$  and consequently the relative contribution of  $s$ - and  $u$ -channels; i.e. the phase  $\alpha$  might differ from zero. In order to demonstrate the influence of the interference term we show in Figs. 5, 6 the coherent sum of  $s(N)$  and  $u(N)$  channels with a 'minus' (i.e.  $\alpha = \pi$ ) interference ( $s + u - int.$ ) (cf. dot-dot-dashed lines). One can see that the situation turns over – for the  $pp \rightarrow pna_0^+$ ,  $pn \rightarrow ppa_0^-$  and  $pn \rightarrow pna_0^0$  reactions the interference becomes destructive, whereas for  $pp \rightarrow ppa_0^0$  the interference is positive. For the  $pp \rightarrow pna_0^+$ ,  $pn \rightarrow ppa_0^-$  and  $pn \rightarrow pna_0^0$  reactions the difference between the interferences with 'plus' and 'minus' sign is about of factor 3-4, however, for the  $pp \rightarrow ppa_0^0$  channel this difference is drastic; i.e. more than two orders of magnitude close to threshold.

As seen from Figs. 5, 6, we get the largest cross section for the  $pp \rightarrow pna_0^+$  isospin channel. For this reaction the

$u$ -channel gives the dominant contribution, the  $s$ -channel cross section is small such that the interference is not so essential as for the  $pp \rightarrow ppa_0^0$  reaction.

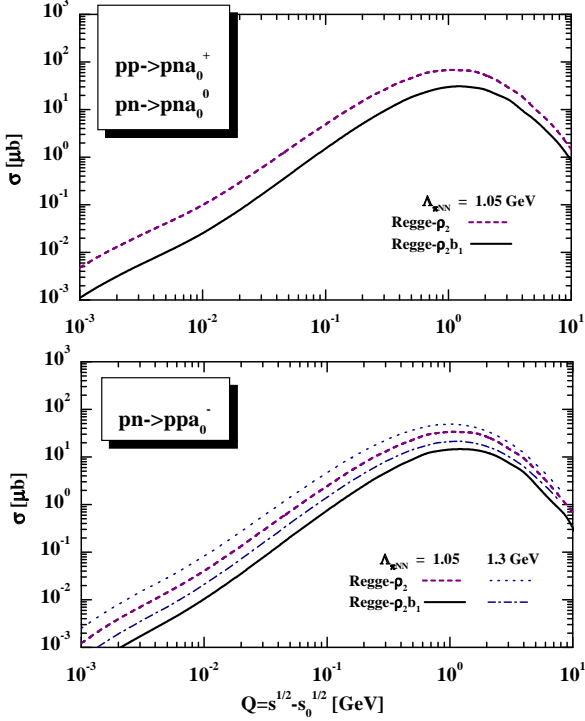


**Fig. 7.** The total cross sections for the reactions  $pp \rightarrow pna_0^+$ ,  $pn \rightarrow pna_0^0$  (upper part) and  $pn \rightarrow ppa_0^-$  (lower part) as a function of  $Q = \sqrt{s} - \sqrt{s_0}$  calculated within the  $\rho_2$  (dashed lines) and  $(\rho_2, b_1)$  (solid lines) Regge exchange model (with FSI) for cut-off parameters  $\Lambda_{\pi NN} = 1.05$  GeV. The dotted and dot-dashed lines in the lower part show the results for  $\Lambda_{\pi NN} = 1.3$  GeV within the  $\rho_2$  and  $(\rho_2, b_1)$  exchanges, respectively.

The result within the Regge model is shown in Fig. 7 for the reactions  $pp \rightarrow pna_0^+$ ,  $pn \rightarrow pna_0^0$  (upper part) and  $pn \rightarrow ppa_0^-$  (lower part) in a wide energy regime for  $Q = 1 \text{ MeV} \div 10 \text{ GeV}$ . The total cross section is calculated with the  $\rho_2$  (dashed lines) and  $(\rho_2, b_1)$  (solid lines) Regge trajectories (with FSI) for a cut-off parameter  $\Lambda_{\pi NN} = 1.05$  GeV. In order to show the influence of the cut-off parameter  $\Lambda_{\pi NN}$  in the Regge model we present in the lower part of Fig. 7 the results for  $\Lambda_{\pi NN} = 1.3$  GeV – the dotted line for  $\rho_2$  exchange and the dot-dashed line for the  $(\rho_2, b_1)$  trajectory. Changing the cut-off  $\Lambda_{\pi NN} = 1.05$  to 1.3 GeV gives a difference of about of factor 2 in the total cross section similar to the results within the effective Lagrangian model (cf. Fig. 3).

As it was already discussed in our previous study [22] an effective Lagrangian model can not be extrapolated to high energies because it predicts the elementary amplitude  $\pi N \rightarrow a_0 N$  rising fast. Therefore, this model can only be employed not far from the threshold. On the other hand, the Regge model is valid at large energies and we have to worry, how close to the threshold we can extrap-

olate corresponding amplitudes. According to duality arguments one can expect that the Regge amplitude can be applied at low energy, too, if the reaction  $\pi N \rightarrow a_0 N$  does not contain essential  $s$ -channel resonance contributions. In this case the Regge model might give a realistic estimate of the  $\pi N \rightarrow a_0 N$  amplitude even near threshold. Anyway, as we have shown in our previous paper [22] the Regge and  $u$ -channel model give quite similar results for the  $\pi^- p \rightarrow a_0^0 n$  cross-section in the near threshold region; some differences in the cross sections of the reactions  $NN \rightarrow NN a_0$  – as predicted by those two models – can be attributed to differences in the isospin factors and effects of  $NN$  antisymmetrization.

## 5 The reaction $NN \rightarrow NN a_0 \rightarrow NN K \bar{K}$

### 5.1 The $K \bar{K}$ and $\pi\eta$ decay channels of the $a_0(980)$

The  $a_0(980)$  meson production has not yet been measured in  $NN \rightarrow NN a_0$  reactions. There are only few  $pp \rightarrow pp K \bar{K}$  and  $pp \rightarrow pn K \bar{K}$  experimental data points. Therefore, it is important to analyse a possible resonance contribution to  $K \bar{K}$  production in the reactions  $NN \rightarrow NN X$ , using the calculated  $NN \rightarrow NN a_0$  amplitudes and the experimental fits obtained for the  $a_0$  resonance mass distribution in the  $K \bar{K}$  decay channel.

The amplitude for the  $a_0(980)$  decays into  $K \bar{K}$  and  $\pi\eta$  modes can be parametrized by the well-known Flatté formula [35] which satisfies both requirements of analyticity and unitarity for the two-channels  $\pi\eta$  and  $K \bar{K}$ .

In the case of the  $a_0(980)$  resonance the mass distribution of the final  $K \bar{K}$  system can be written as a product of the total cross section for  $a_0$  production (with the 'running' mass  $M$ ) in the  $NN \rightarrow NN a_0$  reaction (10) and the Flatté mass distribution function

$$\frac{d\sigma_{K\bar{K}}}{dM^2}(s, M) = \sigma_{a_0}(s, M), \quad (17)$$

$$\times C_F \frac{M_R \Gamma_{a_0 K\bar{K}}(M)}{(M^2 - M_R^2)^2 + M_R^2 \Gamma_{tot}^2(M)}$$

with the total width  $\Gamma_{tot}(M) = \Gamma_{a_0 K\bar{K}}(M) + \Gamma_{a_0 \pi\eta}(M)$ . The partial widths

$$\Gamma_{a_0 K\bar{K}}(M) = g_{a_0 K\bar{K}}^2 \frac{q_{K\bar{K}}}{8\pi M^2},$$

$$\Gamma_{a_0 \pi\eta}(M) = g_{a_0 \pi\eta}^2 \frac{q_{\pi\eta}}{8\pi M^2} \quad (18)$$

are proportional to the decay momenta in the center-of-mass (in case of scalar mesons),

$$q_{K\bar{K}} = \frac{[(M^2 - (m_K + m_{\bar{K}})^2)(M^2 - (m_K - m_{\bar{K}})^2)]^{1/2}}{2M}$$

$$q_{\pi\eta} = \frac{[(M^2 - (m_\pi + m_\eta)^2)(M^2 - (m_\pi - m_\eta)^2)]^{1/2}}{2M}$$

for a meson of mass  $M$  decaying to  $K \bar{K}$  and  $\pi\eta$ , correspondingly. The branching ratios  $Br(a_0 \rightarrow K \bar{K})$  and

$Br(a_0 \rightarrow \pi\eta)$  are given by the integrals of the Flatté distribution over the invariant mass squared  $dM^2 = 2M dM$ :

$$Br(a_0 \rightarrow K\bar{K}) = \int_{m_K+m_{\bar{K}}}^{\infty} \frac{dM}{2M} \frac{2M C_F M_R \Gamma_{a_0 K\bar{K}}(M)}{(M^2 - M_R^2)^2 + M_R^2 \Gamma_{tot}^2(M)}, \quad (19)$$

$$Br(a_0 \rightarrow \pi\eta) = \int_{m_K+m_{\bar{K}}}^{\infty} \frac{dM}{2M} \frac{2M C_F M_R \Gamma_{a_0 \pi\eta}(M)}{(M^2 - M_R^2)^2 + M_R^2 \Gamma_{tot}^2(M)} \quad (20)$$

$$+ \int_{m_\pi+m_\eta}^{m_K+m_{\bar{K}}} \frac{dM}{2M} \frac{2M C_F M_R \Gamma_{a_0 \pi\eta}(M)}{(M^2 - M_R^2 - M_R \Gamma_{a_0 K\bar{K}}(M))^2 + M_R^2 \Gamma_{a_0 \pi\eta}^2(M)}.$$

The parameters  $C_F, g_{K\bar{K}}, g_{\pi\eta}$  have to be fixed under the constraint of the unitarity condition

$$Br(a_0 \rightarrow K\bar{K}) + Br(a_0 \rightarrow \pi\eta) = 1. \quad (21)$$

Choosing the parameter  $\Gamma_0 = \Gamma_{a_0 \pi\eta}(M_R)$  in the interval  $50 \div 100$  MeV as given by the PDG [36], one can fix the coupling  $g_{\pi\eta}$  according to (18). In Ref. [37] a ratio of branching ratios has been reported,

$$r(a_0(980)) = \frac{Br(a_0 \rightarrow K\bar{K})}{Br(a_0 \rightarrow \pi\eta)} = 0.23 \pm 0.05, \quad (22)$$

for  $m_{a_0} = 0.999$  GeV, which gives  $Br(a_0 \rightarrow K\bar{K}) = 0.187$ . Thus, the two other parameters in the Flatté distribution  $C_F$  and  $g_{a_0 K\bar{K}}$  can be found by solving the system of integral equations, for example, Eq. (19) for  $Br(a_0 \rightarrow K\bar{K}) = 0.187$  and the unitarity condition (21). For our calculations we choose either  $\Gamma_{a_0 \pi\eta}(M_R) = 70$  MeV or 50 MeV, which gives two sets of independent parameters  $C_F, g_{a_0 K\bar{K}}, g_{a_0 \pi\eta}$  for a fixed branching ratio  $Br(a_0 \rightarrow K\bar{K}) = 0.187$ :

$$\text{set 1 } (\Gamma_{tot} = 70 \text{ MeV}): \quad (23)$$

$$g_{a_0 K\bar{K}} = 2.297, \quad g_{a_0 \pi\eta} = 2.189, \quad C_F = 0.365$$

$$\text{set 2 } (\Gamma_{tot} = 50 \text{ MeV}): \quad (24)$$

$$g_{a_0 K\bar{K}} = 1.943, \quad g_{a_0 \pi\eta} = 1.937, \quad C_F = 0.354.$$

Note, that for the  $K^+K^-$  or  $K^0\bar{K}^0$  final state one has to take into account an isospin factor for the coupling constant, i.e.  $g_{a_0 K^+K^-} = g_{a_0 K^0\bar{K}^0} = g_{a_0 K\bar{K}}/\sqrt{2}$ , whereas  $g_{a_0 K^+\bar{K}^0} = g_{a_0 K^-\bar{K}^0} = g_{a_0 K\bar{K}}$ .

## 5.2 Numerical results for the total cross section

In the upper part of Fig. 8 we display the calculated total cross section (within parameter *set 1*) for the reaction  $pp \rightarrow pna_0^+ \rightarrow pnK^+\bar{K}^0$  in comparison to the experimental data for  $pp \rightarrow pnK^+\bar{K}^0$  (solid dots) from Ref. [38] as a function of the excess energy  $Q = \sqrt{s} - \sqrt{s_0}$ . The solid lines in Fig. 8 correspond to the incoherent sum of the contributions from  $s(N)$  and  $u(N)$  channels ( $s+u$ ), the dot-dashed lines indicate the coherent sum of  $s(N)$  and  $u(N)$  channels with 'plus' interference ( $s+u+int.$ ), the dot-dot-dashed lines with 'minus' interference ( $s+u-int.$ ). The solid lines with full dots and with open squares represent the results within the  $\rho_2$  and  $(\rho_2, b_1)$  Regge exchange model. The short dashed line shows the 4-body phase space, while the dashed line is the parametrization from Ref. [39].

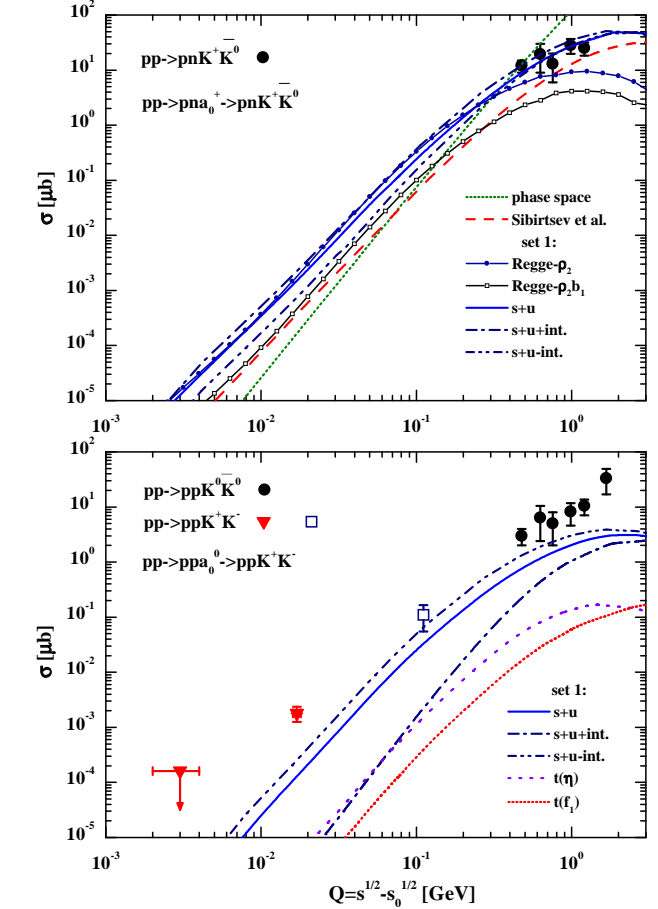


**Fig. 8.** Upper part: the calculated total cross section (within parameter *set 1*) for the reaction  $pp \rightarrow pna_0^+ \rightarrow pnK^+\bar{K}^0$  in comparison to the experimental data for  $pp \rightarrow pnK^+\bar{K}^0$  (solid dots) from Ref. [38] as a function of  $Q = \sqrt{s} - \sqrt{s_0}$ . The solid lines correspond to the incoherent sum of the contributions from  $s(N)$  and  $u(N)$  channels ( $s+u$ ), the dot-dashed lines indicate the coherent sum of  $s(N)$  and  $u(N)$  channels with 'plus' interference ( $s+u+int.$ ), the dot-dot-dashed lines with 'minus' interference ( $s+u-int.$ ). The solid lines with full dots and with open squares represent the results within the  $\rho_2$  and  $(\rho_2, b_1)$  Regge exchange model. The short dashed line shows the 4-body phase space; the dashed line is the parametrization from Ref. [39]. Lower part: the calculated total cross section (within parameter *set 1*) for the reaction  $pp \rightarrow ppa_0^0 \rightarrow ppK^+K^-$  as a function of  $Q = \sqrt{s} - \sqrt{s_0}$  in comparison to the experimental data. The solid dots indicate the data for  $pp \rightarrow ppK^0\bar{K}^0$  from Ref. [38], the open square for  $pp \rightarrow ppK^+K^-$  from Ref. [40]; the full down triangles show the data from Ref. [41].

solid lines with full dots and with open squares present the results within the  $\rho_2$  and  $(\rho_2, b_1)$  Regge exchange model. The short dashed line shows the 4-body phase space, while the dashed line is the parametrization from Sibirtsev et al. [39]. We note, that the cross sections for parameter *set 2* are similar to *set 1* and larger by a factor  $\sim 1.5$ .

In the lower part of Fig. 8 we show the calculated total cross section (within parameter *set 1*) for the reaction

$pp \rightarrow ppa_0^0 \rightarrow ppK^+K^-$  as a function of  $Q = \sqrt{s} - \sqrt{s_0}$  in comparison to the experimental data. The solid dots indicate the data for  $pp \rightarrow ppK^0\bar{K}^0$  from Ref. [38], the open square for  $pp \rightarrow ppK^+K^-$  from the DISTO collaboration [40], the full down triangles show the data from COSY-11 [41].

For the  $pp \rightarrow ppa_0^0 \rightarrow ppK^+K^-$  reaction (as for  $pp \rightarrow ppa_0^0$ ) there is no contribution from meson Regge trajectories;  $s$ - and  $u$ -channels give similar contributions such that their interference according to the OPE model (line  $s+u+int.$ ) is strongly destructive (cf. upper part of Fig. 5). However, even the 'upper limit' for the interference (line  $s+u-int.$ ) is much lower than the COSY experiment near threshold [41]. The  $t(f_1)$  contribution (short dotted line) is practically negligible, while the  $t(\eta)$ -channel (dotted line) is important closer to the threshold, especially in the case of 'plus' interference.

Thus our model gives quite small cross sections for  $a_0^0$  production in the  $pp \rightarrow ppK^+K^-$  reaction which complicates its experimental observation for this isospin channel. The situation looks more promising for the  $pp \rightarrow pna_0^+ \rightarrow pnK^+\bar{K}^0$  reaction since the  $a_0^+$  production cross section is by an order of magnitude larger than the  $a_0^0$  one. Moreover, as has been pointed out with respect to Fig. 5, the influence of the interference is not so strong as for the  $pp \rightarrow ppa_0^0 \rightarrow ppK^+K^-$  reaction.

Here we would like to stress again the limited applicability of the effective Lagrangian model (ELM) at high energies. As seen from the upper part of Fig. 8, the ELM calculations at high energies go through the experimental data, which is not realistic since also other channels contribute to the  $K^+\bar{K}^0$  production in  $pp$  reactions (cf. dashed line from Ref. [39]). Moreover, the ELM calculations are higher than the Regge model predictions which indicates, that the ELM amplitudes at high energies should be reggeized.

### 5.3 Numerical results for the invariant mass distribution

As follows from the lower part of Fig. 8, the  $a_0$  contribution to the  $K^+K^-$  production in the  $pp \rightarrow ppK^+K^-$  reaction near the threshold is hardly seen. With increasing energy the cross section grows up, however, even at  $Q = 0.111$  GeV the 'plus' interference ( $s+u+int.$ ) gives only a few percent contribution to the  $0.11 \pm 0.009 \pm 0.046 \mu\text{b}$  'nonresonant' cross section (without  $\phi \rightarrow K^+K^-$ ) from the DISTO collaboration [40]. On the other hand, the 'minus' interference ( $s+u-int.$ ) gives  $\sim 60\%$  while the incoherent sum of  $s$ - and  $u$ -channels ( $s+u$ ) is  $\sim 30\%$ .

To clarify the situation with the relative contribution of  $a_0^0$  to the total  $K^+K^-$  production in  $pp$  reactions and the influence of the interference term we calculate the  $K^+K^-$  invariant mass distribution for the  $pp \rightarrow ppK^+K^-$  reaction at  $p_{lab} = 3.67$  GeV/c, which corresponds to the kinematical conditions for the DISTO experiment [40]. The differential results are presented in Fig. 9. The upper part shows the calculation within parameter *set 1*,

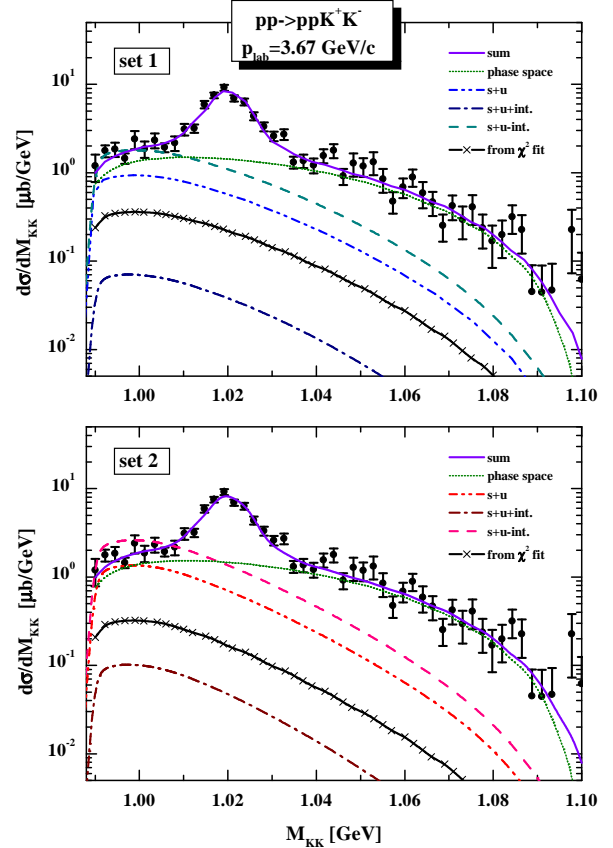


**Fig. 9.** The  $K^+K^-$  invariant mass distribution for the  $pp \rightarrow ppK^+K^-$  reaction at  $p_{lab} = 3.67$  GeV/c. The experimental data are taken from Ref. [40]. The upper part of the plot presents the calculation within parameter *set 1*, whereas the lower part corresponds to *set 2*. The short dotted lines indicate the 4-body phase space, the dot-dot-dashed lines correspond to the incoherent sum of the contributions from  $s(N)$  and  $u(N)$  channels ( $s+u$ ), the dot-dashed lines indicate the coherent sum of  $s(N)$  and  $u(N)$  channels with 'plus' interference ( $s+u+int.$ ), the dashed lines with 'minus' interference ( $s+u-int.$ ). The solid lines with crosses correspond to the coherent sum of  $s(N)$  and  $u(N)$  channels with 'plus' interference and relative phase  $\alpha = 48^\circ$  for *set 1* and  $\alpha = 35^\circ$  for *set 2* according to a  $\chi^2$  fit. The thick solid lines show the sum of all contributions including the decay  $\phi \rightarrow K^+K^-$  (see text).

whereas the lower part corresponds to *set 2*. The dot-dot-dashed lines correspond to the incoherent sum of the contributions from  $s(N)$  and  $u(N)$  channels ( $s+u$ ), the dot-dashed lines indicate the coherent sum of  $s(N)$  and  $u(N)$  channels with 'plus' interference ( $s+u+int.$ ), the dashed lines with 'minus' interference ( $s+u-int.$ ).

One can see from Fig. 9 that, in principle, the  $a_0^0$  might contribute to the  $K^+K^-$  invariant mass spectra at low  $M$ . However, the 'minus' interference model for parameter *set 2* ( $s+u-int.$ ) overestimates the DISTO data at low invariant masses  $M$ , and the same contribution for *set 1* goes through the data without leaving place for 'background', i.e. other channels. On the other hand, the



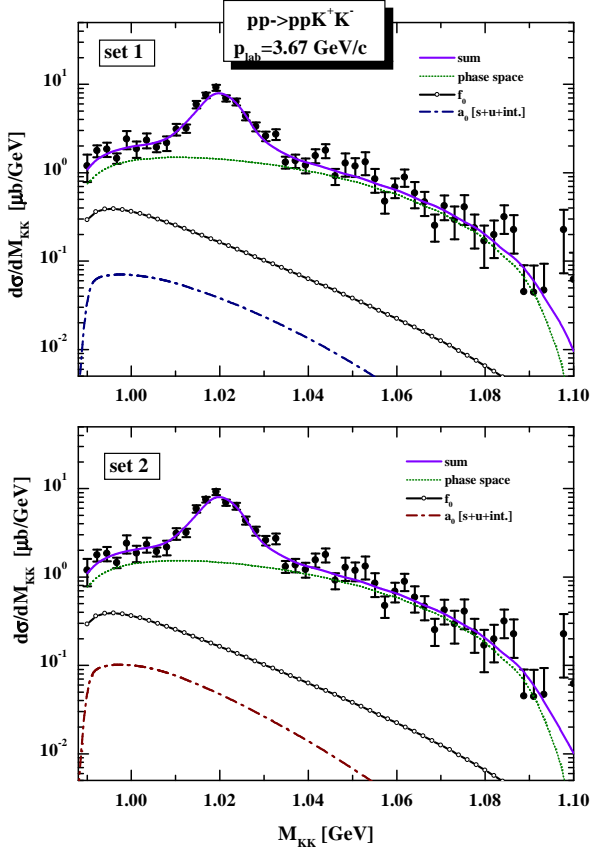


**Fig. 10.** The  $K^+K^-$  invariant mass distribution for the  $pp \rightarrow ppK^+K^-$  reaction at  $p_{lab} = 3.67$  GeV/c. The assignment of the individual lines is the same as in Fig. 9. The solid lines with open circles correspond to the  $f_0$  contribution from Ref. [42]. The experimental data are taken from Ref. [40].

'plus' interference ( $s + u + int.$ ) is not seen at all for both sets of parameters.

One can try to estimate the relative phase of the interference  $\alpha$  from the DISTO data by applying the following procedure: We consider the phase  $\alpha$  as a 'free' parameter which can be fixed by fitting the experimental data with the  $\chi^2$  method, i.e. to minimize (with respect to  $\chi^2$ ) the following function of three parameters  $\alpha, C_1, C_2$ :

$$\frac{d\sigma^{fit}}{dM}(\alpha, C_1, C_2) = \frac{d\sigma^{s+u+int.}}{dM}(\alpha) + C_1 \frac{d\sigma^{4p.s.}}{dM} + C_2 \frac{d\sigma^\phi}{dM}. \quad (25)$$

Here  $d\sigma/dM^{s+u+int.}(\alpha)$  is the contribution attributed to the  $a_0^0$  meson which is calculated as the coherent sum of  $s$ - and  $u$ -channels with phase  $\alpha$ ;  $d\sigma/dM^{4p.s.}$  is the 4-body phase space,  $d\sigma/dM^\phi$  is the  $\phi$  meson contribution taken as a Breit-Wigner distribution with width  $\Gamma_\phi = 4.43$  MeV folded with a gaussian of width 3.4 MeV that corresponds to the experimental mass resolution [40].

The results of the minimization for the two sets of parameters are shown in Fig. 9 as follows: the short dotted lines indicate the 4-body phase space, the solid lines with crosses correspond to the coherent sum of  $s(N)$  and  $u(N)$  channels with 'plus' interference and phase  $\alpha = 48^\circ$  for

set 1 and  $\alpha = 35^\circ$  for set 2. The thick solid lines show the sum of all three contributions including the decay  $\phi \rightarrow K^+K^-$ .

The best  $\chi^2$  fit of the DISTO data clearly indicates a destructive interference between  $s$ - and  $u$ -channels. However, before making final conclusions about the phase  $\alpha$  of the interference term, one has to consider also the contribution from the  $f_0$  scalar meson, i.e. the  $pp \rightarrow pp f_0 \rightarrow ppK^+K^-$  reaction. The  $f_0$  production in  $pp$  reactions has been studied in detail in Ref. [42]. Here we use the result from our previous work [42] and show in Fig. 10 the contribution from the  $f_0$  meson calculated with parameter set A from Ref. [42] as the solid line with open circles ( $f_0$ ).

We find that the  $f_0$  contribution is practically identical in shape and absolute value to the fitted (maximum)  $a_0^0$  contribution (the solid lines with crosses from Fig. 9). This means that there is no 'room' for the  $a_0^0$  contribution in the DISTO data, i.e. the phase  $\alpha$  should be close to zero in line with the OPE model presented in Section 2.

Thus, our present knowledge is summarized in Fig. 10: the  $f_0$  meson gives some contribution to the  $K^+K^-$  invariant mass distribution at low invariant masses  $M$ , that is  $\sim 12\%$  of the total 'nonresonant' cross section from the DISTO collaboration [40]. The  $a_0^0$  meson is practically not seen in  $pp \rightarrow ppK^+K^-$  reactions due to the strong destructive interference between  $s$ - and  $u$ -channels. In this respect the reaction  $pp \rightarrow pnK^+K^0$  seems to be more promising for  $a_0$  measurements as it has been pointed out in the previous subsection.

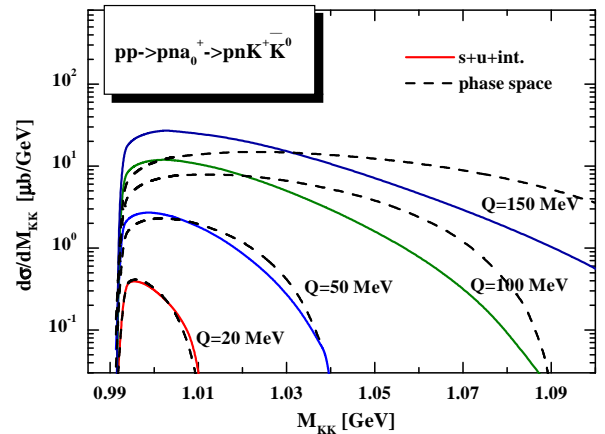


**Fig. 11.** The  $K^+\bar{K}^0$  invariant mass distribution for the  $pp \rightarrow pnK^+\bar{K}^0$  reaction at different  $Q$ . The solid lines describe the  $a_0^+$  resonance contributions. The dashed lines show the invariant mass distributions for 'background' under the assumption that the integrals below the solid and dashed lines are the same for each  $Q$ .

For an experimental determination of the  $a_0^+$  we present the invariant mass distribution of  $K^+\bar{K}^0$  in the reaction  $pp \rightarrow pnK^+\bar{K}^0$  at different  $Q$  (solid lines) in Fig. 11. The dashed lines show the invariant mass distributions for 'background' (i.e. according to phase space) under the assumption that the integrals below the solid and dashed

lines are the same for each  $Q$ . We see that the shape of the solid and dashed lines are practically the same for  $Q \leq 50$  MeV. Noticeable differences between the lines can be found for  $Q \geq 100$  MeV. This means that a separation of the resonance contribution from the background very close to threshold can be done only in the case when the background is small or very well known. In fact, as can be seen from the upper part of Fig. 8, the  $a_0^+$  resonance contribution for  $Q \leq 100$  MeV is larger than the nonresonant cross section as given by the model of Ref. [39] (dashed curve) as well as by the four-body phase space (dotted curve).

## 6 Conclusions

In this work we have estimated the cross sections of  $a_0$  production in the reactions  $pp \rightarrow ppa_0^0$ ,  $pp \rightarrow pna_0^+$ ,  $pn \rightarrow ppa_0^-$  and  $pn \rightarrow pna_0^0$  near threshold and at medium energies. Using an effective Lagrangian approach with one-pion exchange we have analyzed different contributions to the cross section corresponding to  $t$ -channel diagrams with  $\eta(550)$ - and  $f_1(1285)$ -meson exchanges as well as  $s$  and  $u$ -channel graphs with an intermediate nucleon. We additionally have considered the  $t$ -channel Reggeon exchange mechanism. These results have been used to calculate the contribution of  $a_0$  mesons to the cross sections of the reactions  $pp \rightarrow pnK^+\bar{K}^0$  and  $pp \rightarrow ppK^+K^-$ . Due to unfavourable isospin Clebsch-Gordan coefficients as well as rather strong destructive interference of the  $s$ - and  $u$ -channel contributions our model gives quite small cross sections for  $a_0^0$  production in the  $pp \rightarrow ppK^+K^-$  reaction. However, the  $a_0^+$  production cross section in the  $pp \rightarrow pna_0^+ \rightarrow pnK^+\bar{K}^0$  reaction should be larger by an order of magnitude. Therefore the experimental observation of  $a_0^+$  in the reaction  $pp \rightarrow pnK^+\bar{K}^0$  is much more promising than the observation of  $a_0^0$  in the reaction  $pp \rightarrow ppK^+K^-$ . We note in passing that the  $\pi\eta$  decay channel is experimentally more challenging since, due to the larger nonresonant background [43], the identification of the  $\eta$ -meson (via its decay into photons) in a neutral-particle detector is required.

We have also analyzed invariant mass distributions of the  $K\bar{K}$  system in the reaction  $pp \rightarrow pNa_0 \rightarrow pNK\bar{K}$  at different excess energies  $Q$  not far from threshold. Our analysis of the DISTO data on the reaction  $pp \rightarrow ppK^+K^-$  at 3.67 GeV/c has shown that the  $a_0^0$ -meson is practically not seen in  $d\sigma/dM$  at low invariant masses, however, the  $f_0$ -meson gives some contribution. In this respect the possibility to measure the  $a_0^+$  meson in  $d\sigma/dM$  for the reaction  $pp \rightarrow pnK^+\bar{K}^0$  (or  $\rightarrow dK^+\bar{K}^0$ ) looks much more promising not only due to a much larger contribution for the  $a_0^+$ , but also due to the absence of the  $f_0$  meson in this channel.

The authors are grateful to J. Ritman for stimulating discussions and useful suggestions, to V. Baru for providing the parametrization of the FSI enhancement factor and to V. Kleber for a careful reading of the manuscript.

## References

1. G.E. Brown, M. Rho, nucl-th/0103102, Phys. Rep., in press
2. W. Cassing, E. L. Bratkovskaya, Phys. Rep. **308**, 65 (1999)
3. R. Rapp, J. Wambach, Adv. Nucl. Phys. **25**, 1 (2000)
4. F.E. Close et al., Phys. Lett. **B 319**, 291 (1993)
5. M. Genovese et al., Nuovo Cim. **107A**, 1249 (1994)
6. G. Janssen, B. Pierce, K. Holinde and J. Speth, Phys. Rev. D **52**, 2690 (1995)
7. V.V. Anisovich et al., Phys. Lett. **B 355**, 363 (1995)
8. N. A. Törnqvist, Phys. Rev. Lett. **49**, 624 (1982)
9. K. Maltman, ‘Scalar Meson Decay Constants and the Nature of the  $a_0(980)$ ’, Review talk at Hadron-99, Beijing, Aug. 24–28, 1999; hep-ph/0005155; Nucl. Phys. A **675**, 209 (2000)
10. S. Narison, ‘Gluonic Scalar Mesons Hybrids from QCD Spectral Sum Rules’, Review talk at Hadron-99, Beijing, Aug. 24–28, 1999; hep-ph/9909470; Nucl. Phys. Proc. Suppl. **86**, 242 (2000)
11. L. Montanet, Nucl. Phys. B (Proc. Suppl.) **86**, 381 (2000)
12. V.V. Anisovich, L. Montanet, V.N. Nikonov, Phys. Lett. **B 480**, 19 (2000)
13. S. Narison, hep-ph/0012235.
14. N.N. Achasov, S.A. Devyanin, G.N. Shestakov, Phys. Lett. **B88**, 367 (1979)
15. N.N. Achasov, G.N. Shestakov, Phys. Rev. D **56**, 212 (1997)
16. T. Barnes, Phys. Lett. **B 165**, 434 (1985)
17. O. Krehl, R. Rapp, J. Speth, Phys. Lett. **B 390**, 23 (1997)
18. B.O. Kerbikov, F. Tabakin, Phys. Rev. C **62**, 064601 (2000)
19. F. E. Close, A. Kirk, Phys. Lett. **B 489**, 24 (2000)
20. V.Yu. Grishina, L.A. Kondratyuk, M. Büscher, W. Cassing, H. Stroeher, nucl-th/0103081
21. M. Atkinson et al., Phys. Lett. **B 138**, 459 (1984)
22. V.Yu. Grishina, L.A. Kondratyuk, E.L. Bratkovskaya, M. Büscher, W. Cassing, Eur. Phys. J. A **9**, 277 (2000)
23. V. Chernyshev et al., COSY proposal #55 ‘Study of  $a_0^+$  mesons at ANKE’ (1997) *available via www: <http://ikpd15.ikp.kfa-juelich.de:8085/doc/Anke.html>*; L.A. Kondratyuk et al. *Preprint ITEP 18-97*, Moscow (1997)
24. M. Büscher et al., Beam-time request for COSY proposal #55 ‘Study of  $a_0^+$  mesons at ANKE’ (2000) *available via www: <http://ikpd15.ikp.kfa-juelich.de:8085/doc/Anke.html>*
25. M. Büscher et al., Status report for COSY experiment #55 ‘Study of  $a_0^+$  mesons at ANKE’ and Proposal ‘Investigation of neutral scalar mesons  $a_0^0/f_0$  with ANKE’ *available via www: <http://ikpd15.ikp.kfa-juelich.de:8085/doc/Anke.html>*
26. R. Machleidt, K. Holinde, Ch. Elster, Phys. Rep. **149**, 1 (1987)
27. T. Feuster, U. Mosel, Phys. Rev. C **58**, 457 (1998); C **59**, 460 (1999)
28. M. Kirchbach, D. O. Riska, Nucl. Phys. A **594**, 419 (1995)
29. V. Mull, K. Holinde, Phys. Rev. C **51**, 2360 (1995)
30. W.S. Chung, G.Q. Li, C.M. Ko, Nucl. Phys. A **625**, 371 (1997)
31. K. Nakayama, A. Szczurek, C. Hanhart, J. Haidenbauer, J. Speth, Phys. Rev. C **57**, 1580 (1998)

32. V. Baru, A. Kudryavtsev, V. Tarasov, V. Chernyshev, *Preprint ITEP* (1999)
33. A.R. Dzierba, in Proceedings of the Second Workshop on Physics and Detectors for DAΦNE'95, Frascati, 1995, edited by R. Baldini et al., Frascati Physics Series **4**, 99 (1996)
34. V. Baru, A.M. Gasparian, J. Haidenbauer, A.E. Kudryavtsev, J. Speth, nucl-th/0006075, Phys. Atom. Nucl. **64**, 579 (2001)
35. S. Flatté, Phys. Lett. **B 63**, 224 (1976)
36. C. Caso et al. (Particle Data Group), Eur. Phys. J. C **15**, 1 (2000)
37. J. Adomeit et al., Phys. Rev. D **57**, 3860 (1998)
38. Landolt-Börnstein, *New Series*, ed. H. Schopper, I/12 (1988)
39. A.A. Sibirtsev, W. Cassing, C.M. Ko, Z. Phys. A **358**, 101 (1997)
40. F. Balestra et al., Phys. Rev. C **63**, 024004 (2001)
41. C. Quentmeier et al., nucl-ex/0103001
42. E.L. Bratkovskaya, W. Cassing, L.A. Kondratyuk, A. Sibirtsev, Eur. Phys. J. A **4**, 165 (1999)
43. H. Müller, Eur. Phys. J. A **11**, 113 (2001)